ELSEVIER

Contents lists available at ScienceDirect

Materials & Design

journal homepage: www.elsevier.com/locate/matdes



Effect of annealing on mechanical and thermoelectric properties of a Al₂CoCrFeNi high-entropy alloy



Yansong Shi^a, Qinghai Shu^{a,*}, Peter K. Liaw^b, Manman Wang^a, Chien-Lung Teng^c, Haoming Zou^a, Ping Wen^d, Bolin Xu^d, Dongxu Wang^{e,*}, Junfeng Wang^{a,f,*}

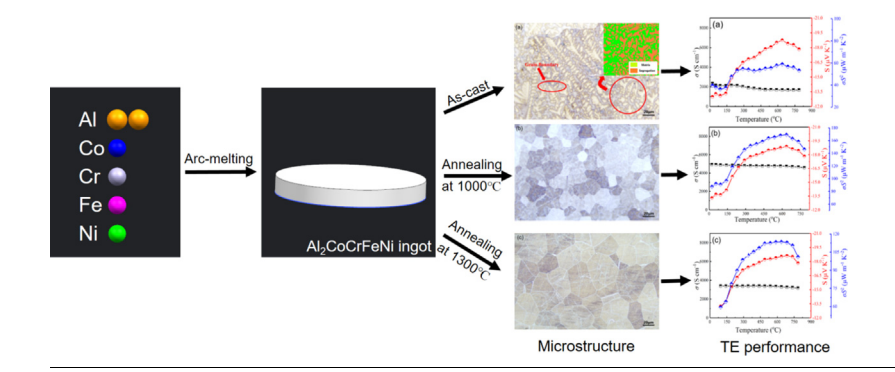
- ^a School of Materials Science & Engineering, Beijing Institute of Technology, Beijing 100081, PR China
- ^b Department of Materials Science and Engineering, The University of Tennessee, Knoxville, TN 37996-2200, USA
- ^c Beijing Energetic Pioneer Natural Science Research Institute, Beijing 100081, PR China
- ^d State-owned Changhong Machinery Factory, GuiLin 541002, PR China
- ^e School of Physics, Beijing Institute of Technology, Beijing 100081, PR China
- ^f State Key Laboratory of Explosion Science and Technology, Beijing Institute of Technology, Beijing 100081, PR China

HIGHLIGHTS

A lightweight and high strength HEAbased TE material Al₂CoCrFeNi is prepared.

- Annealing process affect the microstructure evolution of Al₂CoCrFeNi.
- Microstructure characteristics affect mechanical and thermoelectric properties.

G R A P H I C A L A B S T R A C T



ARTICLE INFO

Article history: Received 11 August 2021 Revised 29 November 2021 Accepted 7 December 2021 Available online 8 December 2021

Keywords: High-entropy alloys Annealing treatment Microstructure evolution Thermoelectric performance

Mechanical properties

ABSTRACT

In this study, a relatively light and high strength high entropy alloy thermoelectric material ($Al_2CoCrFeNi$) for extreme service conditions was prepared by arc melting method. We find that the microstructure of the high entropy alloy (HEA) can be changed by annealing. By the tuning of proper annealing process, the microstructure evolution of the HEA can be adjusted to improve its mechanical and TE properties. Ultimate compressive strength can reach about 1.3 GPa after $1000\,^{\circ}C$ annealing. Fine-grain and precipitation strengthening are the main reasons for the improvement of the mechanical properties. The conductivity, Seebeck coefficient and thermal conductivity are all affected by grain size, precipitates, structural complexity and so on. The present work provides an effective means of preparing and regulating microstructures for the energy-conversion technique, and also supplies a feasible reference for the future development of lightweight, high-strength HEA TE materials.

© 2021 Published by Elsevier Ltd. This is an open access article under the CC BY-NC-ND license (http://creativecommons.org/licenses/by-nc-nd/4.0/).

1. Introduction

Thermoelectric (TE) materials, which have potential uses for green renewable-energy-conversion, employ thermoelectric effects to directly convert thermal and electrical energies without

E-mail addresses: qhshu121@bit.edu.cn (Q. Shu), dadadolindsay@126.com (D. Wang), wjf2015@bit.edu.cn (J. Wang).

^{*} Corresponding authors at: School of Materials Science & Engineering, Beijing Institute of Technology, Beijing 100081, PR China (J. Wang).

polluting the environment [1-3]. They offer an effective solution with good comprehensive social benefits [4].

Many TE materials are being explored for power generation applications, such as GeTe [5], PbTe [6,7], Bi₂Te₃ [8] and silicides [9]. Regular TE materials, such as metallics and conductive polymers, are mainly used for the thermal-energy management at near-room temperature, and have difficulty working at mediumhigh temperatures (about 200 $^{\circ}$ C - 700 $^{\circ}$ C) due to structural evolution and pyrolyzation [10]. Other traditional TE materials focus on semi-conductive elements in the IV or VI groups. As a result, it leads to high density and low mechanical properties. However, it would also be significant to achieve energy harvesting in extreme conditions - for example, aerospace or other military needs - for which a lightweight material with acceptable mechanical performance is also required, in addition to a high-TE efficiency at the medium-high-temperature. Although high-TE performance at medium-high-temperatures has been achieved in half-Heusler alloys [11,12], which often consist of heavy metals or toxic elements, making them as poor candidates for the deployment in the aforementioned fields of specific engineering fields.

Since their discovery by Yeh et al. and Cantor et al. [13,14], high-entropy alloys (HEAs) have been considered as promising materials under severe conditions due to their outstanding mechanical properties and corrosion resistance. Some researchers have studied the microstructure and mechanical properties of high strength HEAs by adding elements [15-18], new processes or new research methods. The high-entropy effect and severe latticedistortion effect are two typical well-known characteristics of HEAs [19-24], of which examples include the phonon-glass electron glass and electron crystal. To be more specific, charge carriers can move freely while the phonons are hindered and scattered, which is beneficial for achieving a high ZT (thermoelectric figure of merit) value as well as a high efficiency in thermal-energy management [25]. Although the high-entropy effect renders HEAs a high band degeneracy, leading to high σ (electrical conductivity) and S (Seebeck coefficient), meanwhile serious lattice distortions exist in $Pb_{0.99-y}Sb_{0.012}SnySe_{1-2x}Te_{x}S_{x}$ [26], $(Cu/Ag)_{2}(S/Se/Te)$, $(Cu/Ag)_{2}(S/Se/Te)$ Ag)₈Ge(Se/Te), (Cu/Ag)(In/Ga)Te₂ and Mn/Ge/Sn/Pb/Te [27] and $(Sn_{0.7}Ge_{0.2}Pb_{0.1})_{0.75}Mn_{0.75}Te$ [28]. The TE performance of HEAs has rarely been investigated in depth in previous reports. Among HEAs, AlCoCrFeNi is an n-type semi-conductor with promising TE performance in the medium-high-temperature region [29,30]. The optimized ZT was reported to be about 0.015 at about 500 °C for Al₂CoCrFeNi [29]. The thermoelectric properties of Al_xCoCrFeNi HEAs were studied via regulating the molar content of Al [31]. However, the origin of this high-TE performance, which involves the evolution of the microstructure and the influence of microstructure on mechanical and thermoelectric properties, has not been well discussed. It remains worthwhile to explore its TE performance with good mechanical behaviors via the thermal treatment.

In the present work, Al₂CoCrFeNi HEAs were successfully prepared via an arc-melting technique. Its density is about 5.2 g/cm³, which is lower than the traditional alloy and semiconductor materials with heavy-metal elements in the medium-high-temperature region mentioned above, and meets the requirements for lightweight use. The microstructural evolution of the Al₂CoCrFeNi HEA has been studied systematically after annealing. Moreover, an appropriate annealing treatment can effectively adjust the microstructure to obtain higher TE and mechanical properties. Furthermore, the variations of microstructural, mechanical, and TE performance with annealing temperature were discussed in detail, using scanning electron microscopy (SEM), transmission electron microscopy (TEM), energy-dispersive X-ray spectrometer (EDS), X-ray diffraction (XRD), and Hall measurement. The current work lays a solid foundation for the develop-

ment of thermal-energy management with lightweight and highstrength HEA semi-conductors.

2. Materials and methods

2.1. Fabrication of HEA

The Al₂CoCrFeNi HEA was prepared via an arc-melting technique. Briefly, Al, Co, Cr, Fe, and Ni element pellets with purities higher than 99.9% (Al 99.999%; Co 99.95%; Cr 99.95%; Fe 99.95%; Ni 99.9%) were purchased from the Zhongnuo Advanced Material (Beijing) Technology Co., Ltd, and alloyed via an arc-melting technique under a high-purity argon atmosphere. The Ti ingot was employed as a getter. The ingot was turned-over at least six times during the alloying process to ensure a uniform microstructure. Then, it was processed into samples of a desired size through a wire-cutting process. Subsequently, annealing processes at 1,000 °C and 1,300 °C for 2 h were utilized to achieve a stable microstructure as well as the desired TE performance of the asprepared HEA in the medium-high-temperature region. All of these samples were grinded with metallographic sandpaper of 100, 200, 400, 600, 800, 1,000, 3,000 and 5,000 meshes and polished with colloidal silica slurry. Finally, the microstructures of the above samples were exposed after treatment by a nitric-acid and ethanol-hybrid solution $(V_{\rm HNO3}/V_{\rm EtOH}=1/5)$ for about 5 s.

2.2. Characterization

2.2.1. Microstructure

The microstructure and chemical composition were first analyzed with SEM, S-4800) using an EDS. The crystal structure was examined via an XRD (Philips X Pert Pro) at 40 kV and 40 mA at a scanning rate of 1/min. from 5° to 90°. The TEM observations were performed, using a 300-keV Tecnai F30 microscope attached to an X-ray energy-dispersive spectrometer (TEM-EDX).

2.2.2. TE and mechanical properties

The compression properties were measured, using a universal testing machine (MTS systems China Co, Ltd, Shanghai, China). Five specimens were measured and the average values were reported. The microhardness was measured, using TH903. The samples were subjected to a load of 5 kg over a load time of 15 s at a load rate of 50 μ m/s. At least seven points were repeatedly tested on each sample, and the average value was used for further investigation. The size of the grains was quantitatively analyzed, using the ImageJ software [32]. A Seebeck coefficient analyzer (ZEM-3) (Advance-Riko, Yokohama, Japan) was used to determine the temperature-dependent Seebeck coefficient and electrical resistivity (1/ σ). The thermal conductivity of the samples was measured by a laser thermal conductivity analyzer (TC-9000H, Ulvac-Riko, Yokohama, Japan), and the cylindrical samples were cut from the center of the ingots with a diameter of 12.7 mm and a thickness of 1.0 mm.

3. 3. Results and discussion

3.1. Phases and microstructures

The XRD patterns of the Al₂CoCrFeNi HEA at different annealing temperatures are shown in Fig. 1. The body-centered-cubic (BCC) phase is found in the as-cast Al₂CoCrFeNi HEA without annealing. And the B2 (ordered BCC) peak also can be observed. After annealing at 1,000 °C, the BCC and B2 peak still exist, and the peak of Cr/Fe phase appears. Additionally, the BCC and B2 phases - characterized as Fe-Cr and Ni-Al phases, respectively - have the same lattice parameters, indicating that they are coherent. With the increase

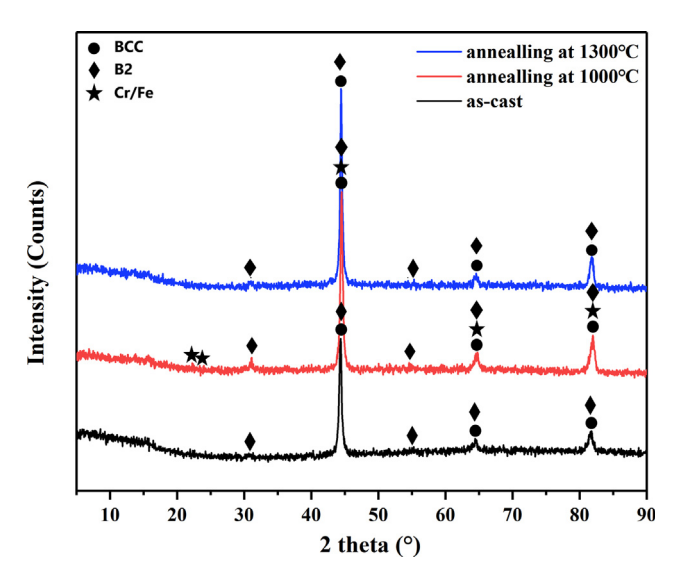


Fig. 1. XRD patterns of the Al₂CoCrFeNi HEA.

of the annealing temperature to 1300 $^{\circ}$ C, no obvious diffraction peak of the Cr/Fe phase was observed.

The optical-microstructure images of the Al₂CoCrFeNi HEA are shown in Fig. 2. In Fig. 2(a), we see that the as-cast Al₂CoCrFeNi HEA has a coarse microstructure and obvious component segregation, resulting in serious inhomogeneity of composition in the grain. The matrix structure is marked in green and the segregation zone is marked in red for clear distinction. It indicate that the microstructures of as-cast Al₂CoCrFeNi HEA comprise of DR (dendrites) and ID (interdendrites) regions. The DR and ID regions are analyzed by SEM-EDS in Fig. 3(a) shows that Co is uniformly distributed in the alloy. The DR regions are mainly composed of Al

and Ni while the ID regions are enriched in Fe and Cr. In Fig. 3 (b), the microstructure of B2 phase is observed by futher SEM analysis in the IR regions, which is consistent with the XRD result.

Phase formation for HEAs can be predicted by calculating the parameters Ω and δ , proposed by Yang et al. [33] Ω represents the competition between enthalpy and entropy, given by

$$\Omega = \frac{T_m \Delta S_{mix}}{|\Delta H_{mix}|} \tag{1}$$

where $\mathbf{T_m} = \sum \mathbf{c_i}(\mathbf{T_m})_i$ is the melting temperature of the alloy, $\mathbf{c_i}$ is the content of different elements, $(T_m)_i$ is the melting point of different elements. $\Delta \mathbf{S}_{\text{mix}} = -\mathbf{R} \sum \mathbf{c_i} \mathbf{lnc_i}$ is the entropy of mixing [19], \mathbf{R} is the gas constant. $\Delta \mathbf{H}_{\text{mix}} = \sum_{i < j} 4\mathbf{c_i}\mathbf{c_j}\Delta \mathbf{H}_{ij}^{\text{mix}}$ is the enthalpy of mixing, $\Delta \mathbf{H}_{ij}^{\text{mix}}$ is the enthalpy of binary mixing. δ represents the atomic size difference, given by

$$\delta = \sqrt{\sum c_{\mathbf{i}} \left(\frac{1 - \mathbf{r}_{\mathbf{i}}}{\bar{\mathbf{r}}}\right)^{2}} \tag{2}$$

where r_i is the radius of the atom, r is the average atomic radius. According to ref. [33], $\Omega \geq 1.1$ and $\delta \leq 6.6$ % should be expected as the criteria for forming high-entropy stabilized solid solution phases. The calculation shows that the parameters of our Al₂CoCrFeNi HEA are $\Omega = 1.3$ and $\delta = 6.6$ %. Therefore, it may tend to be a solid solution. These quantitative predictions are mostly consistent with the empirical data albeit with a few exceptions. In the solidification process of smelting, the solid solution with a simple crystalline structure is formed first. Because the atomic radius of Al is larger than that of other atoms (Al 1.432 Å, Co 1.251 Å, Cr 1.249 Å, Fe 1.241 Å, Ni 1.246 Å [34]), its crystal lattice produces a larger distortion energy and is extremely unstable;

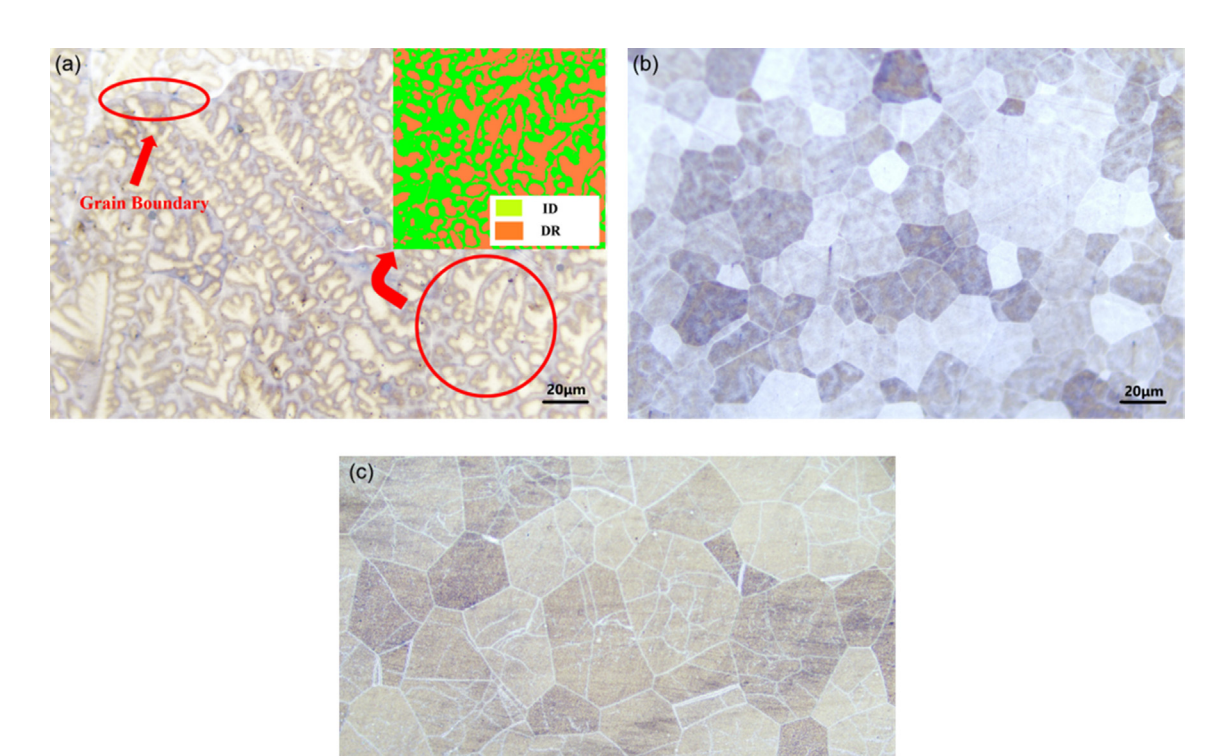


Fig. 2. The OM of Al₂CoCrFeNi (a) as-cast, (b) annealing at 1,000°C, and (c) annealing at 1,300°C.

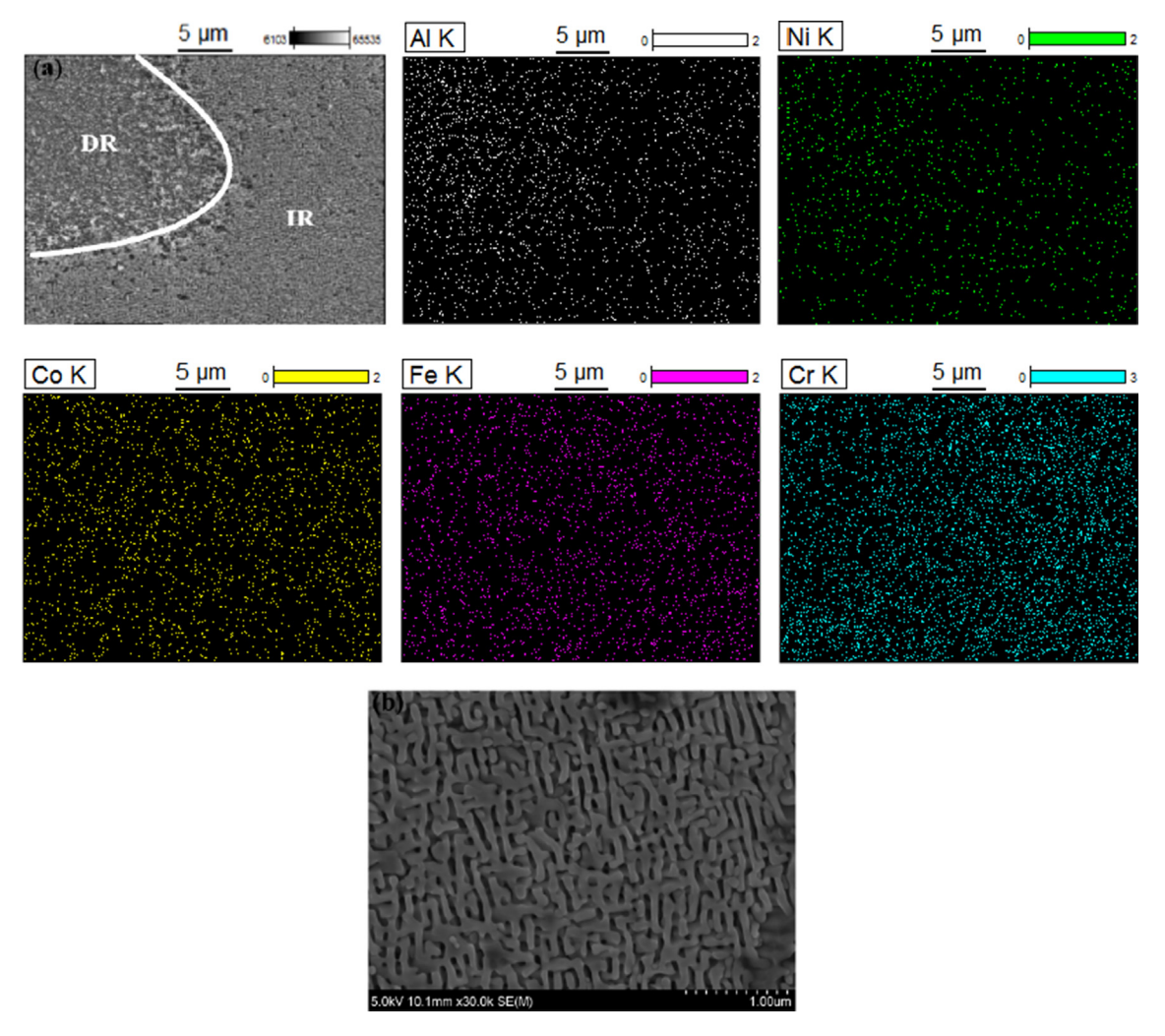


Fig. 3. (a) The SEM-EDS mappings of the as-cast Al₂CoCrFeNi HEA, (b) High magnification SEM in the IR regions.

with the decrease of cooling temperature, the solid solubility of Al decreases and Al precipitates from the solid solution and segregates.

After annealing at 1,000 °C, atoms in the solid-solution alloy diffuse and the Al element is dissolved back, resulting in reduced or even disappearance of inner-grain segregation. The microstructural heterogeneity is weakened and a fine-grain structure is presented. The grains are more complete, the boundary is cleared, and the crystallinity is improved, which is consistent with the increased-crystallinity phenomenon illustrated by the sharper diffraction peak in Fig. 1. Furthermore, under the high magnification of TEM and SEM in Fig. 4(a), it can be observed that there are fine spherical particles with a dispersion distribution in the alloy and amplitude-modulated decomposed structures in the matrix are similar to that in the as-cast sample. The corresponding selected-area electron-diffraction (SAED) pattern in the (100) zone axis is given in the inset. We can infer that the amplitudemodulated decomposed structure is in the B2 (ordered BCC) phase, and the SAED shows super-lattice diffraction of the B2 phase, which is consistent with the XRD result. The amplitudemodulated decomposed structure is a characteristic feature of spinodal decomposition and should be formed by periodiccomposition modulations [35,36]. Through XRD in Fig. 1 and TEM-EDX in Fig. 4, we verify that the dispersed fine spherical particles are precipitates mainly containing Cr and Fe elements. Due to the increase of the annealing temperature to 1,300 $^{\circ}$ C, the atoms' diffusion ability is improved, promoting mutual diffusion between metal elements. As presented in Fig. 4(b), it is difficult to observe the spherical Cr/Fe. Most of them are likely to dissolve in the matrix or migrate, which also explains that their corresponding diffraction peaks are not obvious in XRD. The disappearance of dispersed precipitates eliminates the pinning effect on the grain-boundary expansion. In order to reduce the free energy at the interface, the grains merge with each other and grow up, resulting in an increase in grain size.

3.2. Mechanical properties

To study the effects of annealing treatment upon mechanical properties, uniaxial compression and hardness tests are performed. Fig. 5 shows the microhardness of the Al₂CoCrFeNi HEAs. The microhardness of the as-cast Al₂CoCrFeNi HEA is about 482 Hv. After annealing at 1,000 °C, this microhardness is increased to about 516 Hv. When the annealing temperature is 1,300 °C, the microhardness of the alloy decreases to about 467 Hv. The compressive stress-strain curves of the Al₂CoCrFeNi HEAs are illustrated in Fig. 6. The ultimate compressive strength of the as-cast Al₂CoCrFeNi HEA is about 1.21 GPa, and the elongation is about 7.55%. Compared with other elements in the alloy, the atomic radius of Al is larger, causing serious lattice distortion

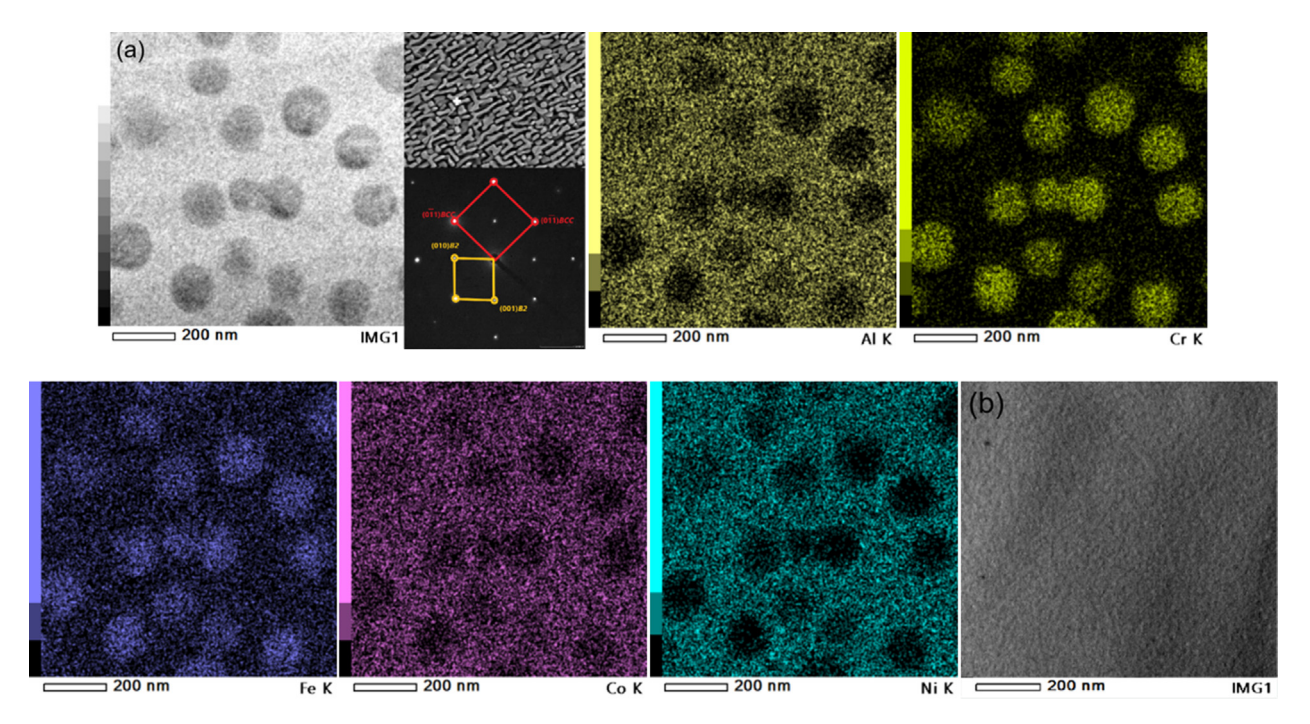


Fig. 4. (a) The TEM-EDX mappings of the Al_2 CoCrFeNi HEA annealed at 1,000°C. The inset shows the micrograph of an amplitude-modulated decomposition structure in the matrix and the indexed SAED pattern in the (100) zone axis, the super-lattice diffractions belonging to the B2 structure are indicated by yellow color, (b) The TEM micrograph of the HEA annealed at 1,300°C. (For interpretation of the references to color in this figure legend, the reader is referred to the web version of this article.)

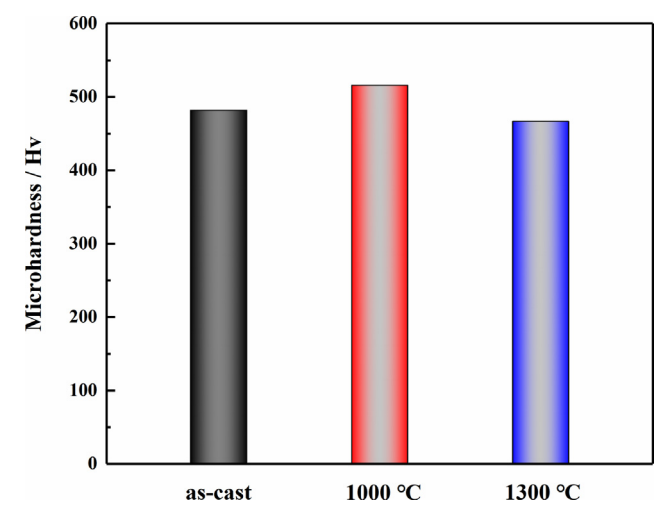


Fig. 5. Microhardness of Al₂CoCrFeNi HEAs.

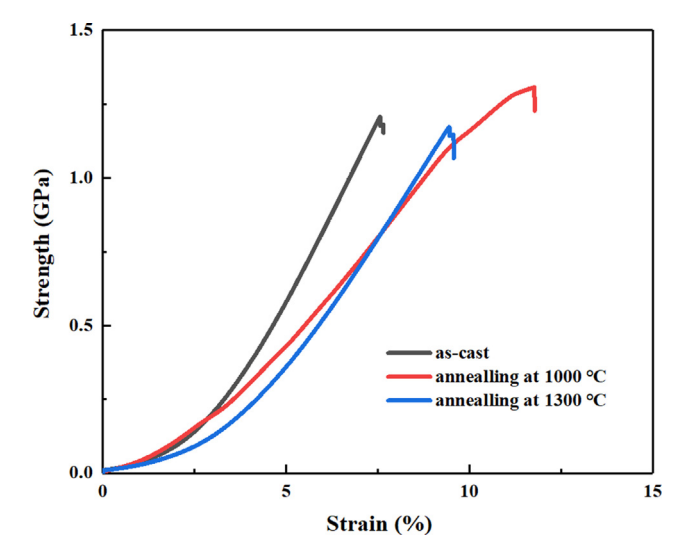


Fig. 6. Compressive stress-strain curves of Al₂CoCrFeNi HEAs.

and increasing the resistance to dislocation movement. Therefore, the as-cast alloy has good strength but poor plasticity due to the large grain size and inhomogeneous structure. When the annealing temperature is 1,000 °C, the ultimate compressive strength increases to 1.30 GPa, and the elongation is about 12.06%. Because annealing treatment accelerates the diffusion of atoms, the defects caused by alloy casting are eliminated and the lattice distortion and internal stress are reduced. However, according to the Hall-Petch formula [37], the finer the grain, the higher the strength achieved. In addition, the dispersed fine particles lead to precipitation strengthening, which causes the strength and hardness to increase rather than decrease after annealing. According to the interaction between moving dislocations and precipitates, the precipitation-strengthening mechanism can be divided into

Orowan bending and particle shear. The Orowan mechanism generally occurs when particles are larger or incoherent with the matrix whereas the shear mechanism mainly occurs when particles are smaller and incoherent. For coherent precipitation, the increase of strength is mainly caused by three factors: coherent strengthening ($\Delta\sigma_{cs}$), dislocation strengthening ($\Delta\sigma_{ms}$), and sequential strengthening ($\Delta\sigma_{os}$) [38]. The first two strengthening processes ($\Delta\sigma_{cs}$ and $\Delta\sigma_{ms}$) occur before the dislocation shear precipitates, while the second strengthening process ($\Delta\sigma_{os}$) takes place during precipitation of the dislocation shear. In this case, the larger the value of ($\Delta\sigma_{cs} + \Delta\sigma_{ms}$) or $\Delta\sigma_{os}$, the greater the total strength increment expected from the shear mechanism. The equations that can be used to calculate these strength increments are [39-41]:

$$\Delta\sigma_{CS} = M * \alpha_{\varepsilon} * (G\varepsilon_C)^{\frac{3}{2}} * \sqrt{\frac{rf}{0.5Gb}} \Delta\sigma_{MS}$$

$$= M * 0.0055 * (\Delta G)^{\frac{3}{2}} * \sqrt{\frac{2f}{G}} * (\frac{r}{b})^{\frac{3m}{2} - 1}$$
(4)

$$\Delta\sigma_{\text{OS}} = M*0.81*\frac{\gamma_{\text{apd}}}{2b}*\sqrt{\frac{3\pi f}{8}} \eqno(5)$$

where M = 2.73 for the BCC structure (Taylor Factor), $\alpha_{\rm E} = 2.6$ (a constant), m = 0.85 (a constant), $\varepsilon_c = 2\varepsilon/3$, the constrained lattice misfit. G and ΔG are the shear modulus of the matrix and the shear modulus mismatch between the precipitates and the matrix, respectively; b is the Burgers vector; r is the average particle size; f is the volume fraction of the precipitates; and Υ_{apb} is the anti-phase boundary energy of the precipitates. The microstructure of the alloy annealed at 1,000 °C is finer and more uniform, and the amount of coordinated deformation in the microstructure is increased, improving the alloy's plasticity. When the annealing temperature is 1,300 °C, the grain size increases to a certain extent, the strength decreases to 1.16 GPa, and the elongation decreases to 9.36%. Compared with the as-cast alloy, annealing at 1,300 °C reduces the lattice distortion and internal stress, resulting in a decrease of the strength and microhardness but an improvement of the plasticity. The grain size is larger than the case for annealing at 1.000 °C and the coordination-deformation ability is poor under the action of force. Hence, the plasticity of the 1,300 °C-annealed alloy is lower than that of the 1,000 °C-annealed alloy. A comparison of the strength and density of Al₂CoCrFeNi HEA with other materials is given in Fig. 7 [42]. Obviously, the strength of Al₂CoCrFeNi HEA is higher than that of most other materials, much higher than that of typical state-of-the-art bulk thermoelectric materials. And the density of Al₂CoCrFeNi HEA is lower.

3.3. Electrical conductivity

The TE performance of a certain semi-conductive material can be calculated using $ZT = \sigma S^2 T/\kappa$, of which σ , S, κ , and T are the electrical conductivity, Seebeck coefficient, thermal conductivity, and absolute temperature, respectively. It is indispensable to obtain a high-TE performance with a high power factor ($PF = \sigma S^2$) and a suppressed κ (which has carrier thermal conductivity $\kappa_{\rm e}$ and lattice thermal conductivity $k_{\rm latt}$ components). Ideal thermoelectric materials should possess a high Seebeck coefficient, high electrical con-

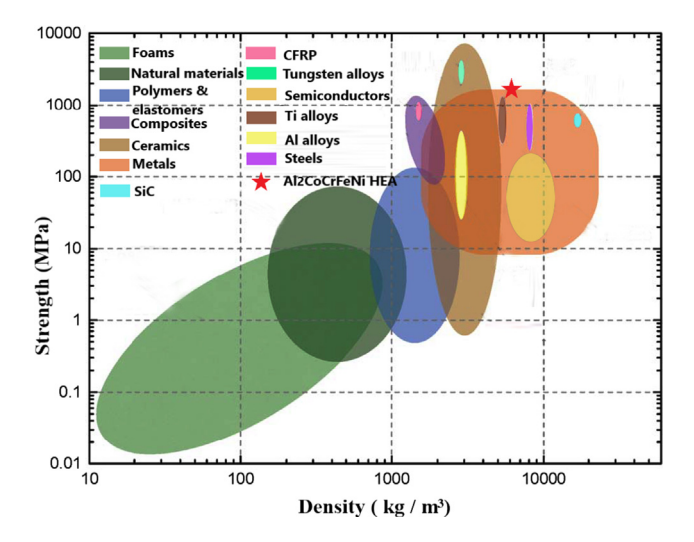


Fig. 7. Ashby plot of strength vs. density for engineering materials. (Yield strength for metals and polymers,tear strength for elastomers, compressive strength for ceramics, and tensile strength for composites.)

ductivity, and low thermal conductivity. However, it is extremely difficult to satisfy these three parameters simultaneously since they are intrinsically intercorrelated. For example, a low carrier concentration leads to a large Seebeck coefficient but also results in low electrical conductivity. Furthermore, material characteristics which result in low thermal conductivity usually result in low electrical conductivity [43].

The conductivity, Seeback coefficient, and PF of the as-cast and annealed alloys are shown in Fig. 8. These parameters are closely related to changes in temperature. It can be seen from the change of the conductivity data that the conductivities of both the as-cast and annealed samples present trends of slight increase with the increase of temperature. As a BCC structure with high Al content, the conductivity of HEA increases with the increase of temperature, which is consistent with the latest research results, higher peak of the density of states is found in the BCC HEAs near the Fermi leve [28]. Small changes in the main phase composition in the microstructure will affect the value of the conductivity [26], the formation of the second phase structure in thermoelectric materials will reduce the lattice conductivity [44], and the uneven distribution of the microstructure in the as-cast alloy and the existence of second phase segregation in the grain will affect the movement of charge carriers (electrons in the metal), leading to a low conductivity. Compared with other samples, the HEA annealed at 1,000 °C possess a high electric conductivity, which is because a large number of fine precipitates are dispersed in the microstructure. These compounds may exhibit good electrical conductivity, which is conducive to the formation of new conductive grids. However, the mechanism needs to be further confirmed. Additionally, the precipitation purifies the matrix to guarantee the conductivity [45].

3.4. Seebeck coefficient

The change in the Seebeck coefficient of the alloy is shown by the red curve in Fig. 8. The positive and negative values of the Seebeck coefficient represent different modes of electron diffusion. The Seebeck coefficients of both as-cast and annealed alloys are negative, indicating that electron transport from the hot end to the cold end is the main mode of electron diffusion. Moreover, due to bipolar conduction, the Seebeck coefficient is basically and directly proportional to the temperature, since noticeable minority carriers would be excited at high temperatures [46]. There is an obvious segregated second phase in the as-cast structure, and the formation of the second phase in the thermoelectric material will introduce a potential barrier, hindering the transition of lowenergy carriers [47,48] and resulting in a lower Seebeck coefficient in the as-cast sample, compared with the annealed one. Additionally, the mechanism of microstructure control of HEAs with band structures needs to be further studied to obtain a satisfactory Seebeck coefficient and to improve the thermoelectric properties of the material.

3.5. Thermal conductivity

As shown in Fig. 9, the thermal conductivity (κ) of as-cast and annealed HEAs increases along with the temperature, but the thermal conductivity of the HEA annealed at 1,000 °C is the lowest overall value. This is because low-dimensional thermoelectric materials follow the size effect, through which the mean free path of phonons can be reduced, thus reducing the lattice's thermal conductivity [49]. At the same time, the large number of spherical Cr/Fe precipitates increase the complexity of the crystal structure. This complexity and the small grain size can enhance the scattering of long-wave phonons. Scattering of phonons results in low thermal conductivity [50]. From the microstructural analysis

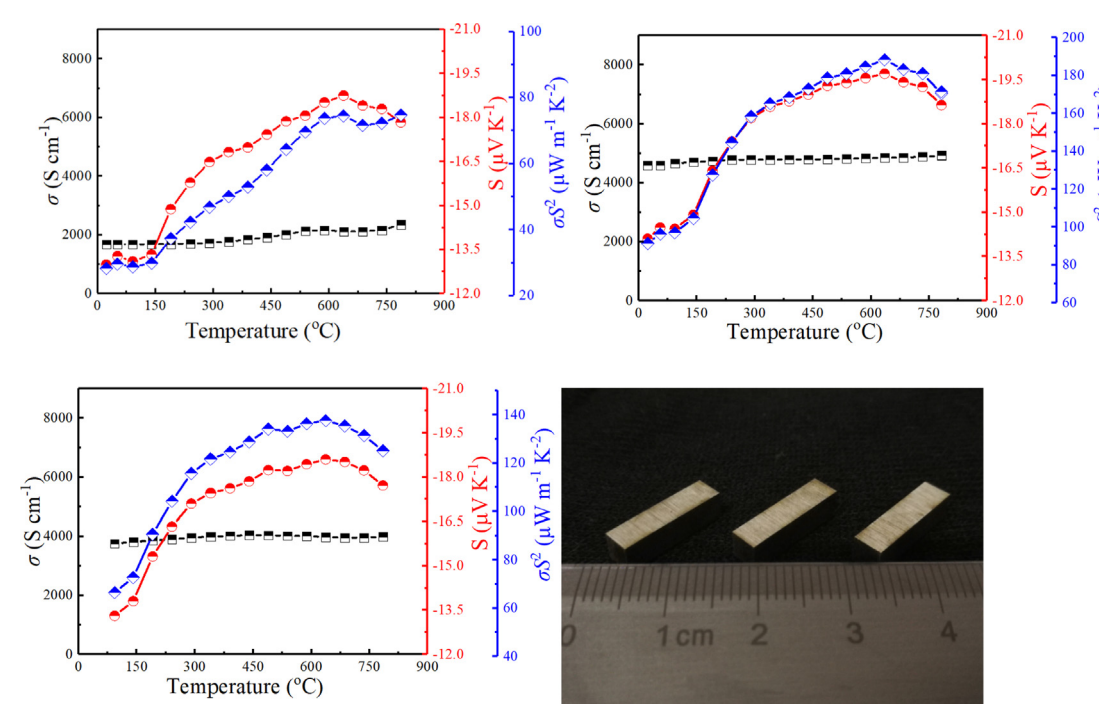


Fig. 8. TE performance of Al₂CoCrFeNi HEAs (a) as-cast, (b) anneal at 1,000°C, (c) anneal at 1,300°C.

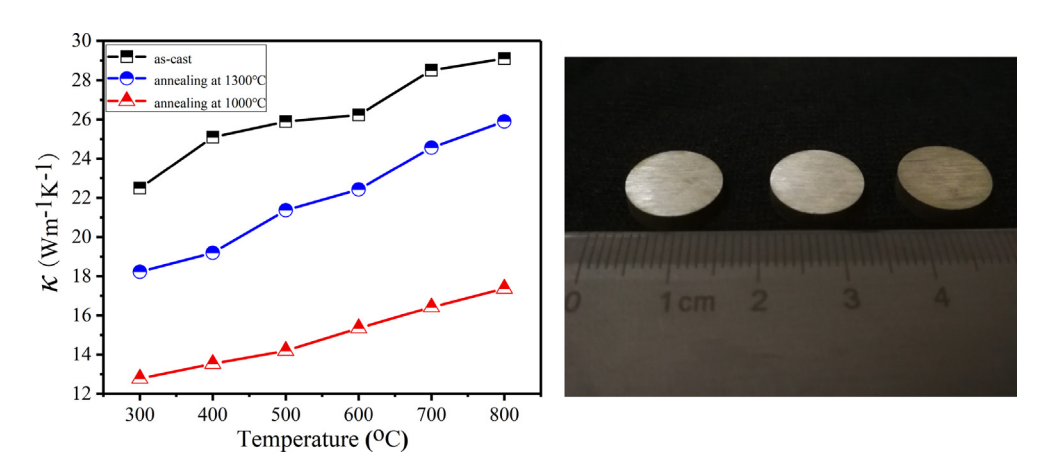


Fig. 9. Thermal conductivity of Al₂CoCrFeNi HEAs.

above, it can be seen that the HEAs in the as-cast state and annealed at 1,300 $^{\circ}$ C have a large grain size, and that the HEA annealed at 1,000 $^{\circ}$ C has the smallest grain size and the lowest lattice thermal conductivity, which is consistent with the grain size and thermal conductivity of all samples [51].

4. Conclusion

The effect of annealing treatment on microstructure and properties of the lightweight Al₂CoCrFeNi HEA is explored. By the tuning of proper annealing process, the microstructure evolution of the HEA can be adjusted to improve its mechanical and TE properties. Fine-grain and precipitation strengthening are the main reasons for the improvement of the mechanical properties. The conductivity, Seebeck coefficient and thermal conductivity are all affected by grain size, precipitates, structural complexity and so on. Facing increasingly complex and harsh application environments for TE materials, the present work provides an effective means of preparation of HEA-based TE material by regulating its

microstructure for the energy-conversion, and also provides a feasible reference for the development of high-entropy TE materials with lightweight and high strengths in the future.

Declaration of Competing Interest

The authors declare that they have no known competing financial interests or personal relationships that could have appeared to influence the work reported in this paper.

Acknowledgement

This work was financially supported by the Fundamental Research Funds for the Central Universities (2020CX01037). P.K.L. appreciates the support of the National Science Foundation under grants of DMR-1611180 and 1809640 and the project numbers of W911NF-13-1-0438 and W911NF-19-2-0049.

References

- [1] X.-L. Shi, J. Zou, Z.-G. Chen, Advanced thermoelectric design: from materials and structures to devices, Chem. Rev. 120 (15) (2020) 7399–7515, https://doi. org/10.1021/acs.chemrev.0c00026.
- [2] G. Tan, L.-D. Zhao, M.G. Kanatzidis, Rationally designing high-performance bulk thermoelectric materials, Chem. Rev. 116 (19) (2016) 12123–12149, https://doi.org/10.1021/acs.chemrev.6b00255.
- [3] J.-S. Rhyee, K.H. Lee, S.M. Lee, E. Cho, S.I. Kim, E. Lee, Y.S. Kwon, J.H. Shim, G. Kotliar, Peierls distortion as a route to high thermoelectric performance in In₄Se₃₋₈ crystals, Nature 459 (7249) (2009) 965–968, https://doi.org/10.1038/nature08088.
- [4] R. Kroon, D.A. Mengistie, D. Kiefer, J. Hynynen, J.D. Ryan, L. Yu, C. Müller, Thermoelectric plastics: from design to synthesis, processing and structureproperty relationships, Chem. Soc. Rev. 45 (22) (2016) 6147–6164, https://doi. org/10.1039/C6CS00149A.
- [5] N. Madar, T. Givon, D. Mogilyansky, Y. Gelbstein, High thermoelectric potential of Bi₂Te₃ alloyed GeTe - rich phases, J. Appl. Phys. 120 (3) (2016) 035102, https://doi.org/10.1063/1.4958973.
- [6] Y. Sadia, T. Ohaion-Raz, O. Ben-Yehuda, M. Korngold, Y. Gelbstein, Criteria for extending the operation periods of thermoelectric converters based on IV-VI compounds, J. Solid State Chem. 241 (2016) 79–85, https://doi.org/10.1016/j. issc.2016.06.006.
- [7] D. Ben-Ayoun, Y. Sadia, Y. Gelbstein, High temperature thermoelectric properties evolution of Pb₁-xSn_xTe based alloys, J. Alloys Compd. 722 (2017) 33–38, https://doi.org/10.1016/j.jallcom.2017.06.075.
- [8] O. Meroz, D. Ben-Ayoun, O. Beeri, Y. Gelbstein, Development of Bi₂Te_{2.4}Se_{0.6} Alloy for Thermoelectric Power Generation Applications, J. Alloys Compd. 679 (2016) 196–201, https://doi.org/10.1016/j.jallcom.2016.04.072.
- [9] Y. Sadia, N. Madar, I. Kaler and Y. Gelbstein, Thermoelectric properties of the quasi-binary MnSi_{1,73}-FeSi₂ system, J. Electron. Mater. 44(6) (2015) 1637-1643. doi: 10.1007/s11664-014-3500-z
- [10] Q. Zhang, Y. Sun, W. Xu, D. Zhu, Organic thermoelectric materials: emerging green energy materials converting heat to electricity directly and efficiently, Adv. Mater. 26 (40) (2014) 6829–6851, https://doi.org/10.1002/adma. v26.4010.1002/adma.201305371.
- [11] S. Chen, Z. Ren, Recent progress of half-Heusler-for moderate temperature thermoelectric applications, Mater. Today 16 (10) (2013) 387–395, https://doi. org/10.1016/j.mattod.2013.09.015.
- [12] S. Anand, M. Wood, Y.i. Xia, C. Wolverton, G.J. Snyder, Double half-Heuslers, Joule 3 (5) (2019) 1226–1238, https://doi.org/10.1016/j.joule.2019.04.003.
- [13] J.-W. Yeh, S.-K. Chen, S.-J. Lin, J.-Y. Gan, T.-S. Chin, T.-T. Shun, C.-H. Tsau, S.-Y. Chang, Nanostructured high-entropy alloys with multiple principal elements: novel alloy design concepts and outcomes, Adv. Eng. Mater. 6 (5) (2004) 299–303, https://doi.org/10.1002/(ISSN)1527-264810.1002/adem.v6:510.1002/adem.200300567
- [14] B. Cantor, I.T.H. Chang, P. Knight, A.J.B. Vincent, Microstructural development in equiatomic multicomponent alloys, Mater. Sci. Eng.: A 375-377 (2004) 213-218. doi: 10.1016/j.msea.2003.10.257
- [15] Y. Dong, K. Zhou, Y. Lu, X. Gao, T. Wang, T. Li, Effect of vanadium addition on the microstructure and properties of AlCoCrFeNi high entropy alloy, Mater. Des. 57 (2014) 67–72, https://doi.org/10.1016/j.matdes.2013.12.048.
- [16] Z. Hu, Y. Zhan, G. Zhang, J. She, C. Li, Effect of rare earth Y addition on the microstructure and mechanical properties of high entropy AlCoCrCuNiTi alloys, Mater. Des. 31 (3) (2010) 1599–1602, https://doi.org/10.1016/ j.matdes.2009.09.016.
- [17] J. Chen, P. Niu, Y. Liu, Y. Lu, X. Wang, Y. Peng, J. Liu, Effect of Zr content on microstructure and mechanical properties of AlCoCrFeNi high entropy alloy, Mater. Des. 94 (2016) 39–44, https://doi.org/10.1016/j.matdes.2016.01.033.
- [18] M. Vaidya, A. Prasad, A. Parakh, B.S. Murty, Influence of sequence of elemental addition on phase evolution in nanocrystalline AlCoCrFeNi: Novel approach to alloy synthesis using mechanical alloying, Mater. Des. 126 (2017) 37–46, https://doi.org/10.1016/j.matdes.2017.04.027.
- [19] E.P. George, D. Raabe, R.O. Ritchie, High-entropy alloys, Nat. Rev. Mater. 4 (8) (2019) 515–534, https://doi.org/10.1038/s41578-019-0121-4.
- [20] Y.D. Wu, Y.H. Cai, X.H. Chen, T. Wang, J.J. Si, L. Wang, Y.D. Wang, X.D. Hui, Phase composition and solid solution strengthening effect in TiZrNbMoV highentropy alloys, Mater. Des 83 (2015) 651–660, https://doi.org/10.1016/ j.matdes.2015.06.072.
- [21] C. Lee, Y.i. Chou, G. Kim, M.C. Gao, K.e. An, J. Brechtl, C. Zhang, W. Chen, J.D. Poplawsky, G. Song, Y. Ren, Y.-C. Chou, P.K. Liaw, Lattice-Distortion-Enhanced Yield Strength in a Refractory High-Entropy Alloy, Adv. Mater. 32 (49) (2020) 2004029, https://doi.org/10.1002/adma.v32.4910.1002/adma.202004029.
- [22] W.P. Chen, Z.Q. Fu, S.C. Fang, H.Q. Xiao, D.Z. Zhu, Alloying behavior, microstructure and mechanical properties in a FeNiCrCo_{0.3}Al_{0.7} high entropy alloy, Mater. Des. 51 (2013) 854–860, https://doi.org/10.1016/ j.matdes.2013.04.061.
- [23] C. Zhang, F. Zhang, H. Diao, M.C. Gao, Z. Tang, J.D. Poplawsky, P.K. Liaw, Understanding phase stability of Al-Co-Cr-Fe-Ni high entropy alloys, Mater. Des. 109 (2016) 425–433, https://doi.org/10.1016/j.matdes.2016.07.073.
- [24] Q. Ding, Y. Zhang, X. Chen, X. Fu, D. Chen, S. Chen, L. Gu, F. Wei, H. Bei, Y. Gao, M. Wen, J. Li, Z.e. Zhang, T. Zhu, R.O. Ritchie, Q. Yu, Tuning element distribution, structure and properties by composition in high-entropy alloys, Nature 574 (7777) (2019) 223–227, https://doi.org/10.1038/s41586-019-1617-1.

- [25] L.-D. Zhao, V.P. Dravid, M.G. Kanatzidis, The panoscopic approach to high performance thermoelectrics, Energy Environ. Sci. 7 (1) (2014) 251–268, https://doi.org/10.1039/C3EE43099E.
- [26] B. Jiang, Y. Yu, J. Cui, X. Liu, L. Xie, J. Liao, Q. Zhang, Y.i. Huang, S. Ning, B. Jia, B. Zhu, S. Bai, L. Chen, S.J. Pennycook, J. He, High-entropy-stabilized chalcogenides with high thermoelectric performance, Science 371 (6531) (2021) 830–834, https://doi.org/10.1126/science:abe1292.
- [27] R. Liu, H. Chen, K. Zhao, Y. Qin, B. Jiang, T. Zhang, G. Sha, X. Shi, C. Uher, W. Zhang, L. Chen, Entropy as a gene-like performance indicator promoting thermoelectric materials, Adv. Mater. 29 (38) (2017) 1702712, https://doi.org/10.1002/adma.201702712.
- [28] L. Hu, Y. Zhang, H. Wu, J. Li, Y.u. Li, M. Mckenna, J. He, F. Liu, S.J. Pennycook, X. Zeng, Entropy engineering of SnTe: multi-principal-element alloying leading to ultralow lattice thermal conductivity and state-of-the-art thermoelectric performance, Adv. Energy Mater. 8 (29) (2018) 1802116, https://doi.org/10.1002/aenm.v8.2910.1002/aenm.201802116.
- [29] S. Shafeie, S. Guo, Q. Hu, H. Fahlquist, P. Erhart, A. Palmqvist, High-entropy alloys as high-temperature thermoelectric materials, J. Appl. Phys. 118 (18) (2015) 184905, https://doi.org/10.1063/1.4935489.
- [30] W.Q. Dong, Z. Zhou, L.J. Zhang, M.D. Zhang, P.K. Liaw, G. Li, R.P. Liu, Effects of Y, GdCu, and Al addition on the thermoelectric behavior of CoCrFeNi high entropy alloys, Metals 8 (2018) 781, https://doi.org/10.3390/met8100781.
- [31] M.A.A. Hasan, J. Wang, S. Shin, D.A. Gilbert, P.K. Liaw, N. Tang, W.L. Namila, L. Liyanage, L. Santodonato, N.P.B. DeBeer-Schmitt, Effects of Aluminum Content on Thermoelectric Performance of Al_xCoCrFeNi High-Entropy Alloys, J. Alloys Compd. 883 (2021), https://doi.org/10.1016/j.jallcom.2021.160811 160811.
- [32] Y. Shi, Q. Shu, S. Zhao, H. Zou, S. Jin, K. Chen, L. Li, X. Lv, Effect of controlled rolling temperature on microstructure and properties of Mg-9Li-1Zn alloy sheet, J. Alloys Compd. 835 (2020) 155296, https://doi.org/10.1016/ i.jallcom.2020.155296.
- [33] X. Yang, Y. Zhang, Prediction of high-entropy stabilized solid-solution in multicomponent alloys, Mater Chem Phys. 132 (2-3) (2012) 233–238, https://doi. org/10.1016/j.matchemphys.2011.11.021.
- [34] S. Guo, C.T. Liu, Phase stability in high entropy alloys: Formation of solid-solution phase or amorphous phase, Progress in Natural Science: Materials International 21 (6) (2011) 433–446, https://doi.org/10.1016/S1002-0071(12) 60080-X.
- [35] L.J. Santodonato, Y. Zhang, M. Feygenson, C.M. Parish, M.C. Gao, R.J. Weber, J.C. Neuefeind, Z. Tang, P.K. Liaw, Deviation from high-entropy configurations in the atomic distributions of a multi-principal-element alloy, Nat. Commun. 6 (2015) 5964, https://doi.org/10.1038/ncomms6964.
- [36] W.R. Wang, W.L. Wang, S.C. Wang, Y. Tsai, C. Lai, J. Yeh, Effects of Al addition on the microstructure and mechanical property of Al_xCoCrFeNi high-entropy alloys, Intermetallics 26 (2012) 44–51, https://doi.org/10.1016/j. intermet.2012.03.005.
- [37] A. Loucif, R.B. Figueiredo, T. Baudin, F. Brisset, R. Chemam, T.G. Langdon, Ultrafine grains and the Hall-Petch relationship in an Al-Mg-Si alloy processed by high-pressure torsion, Mater. Sci. Eng. A 532 (2012) 139–145, https://doi. org/10.1016/j.msea.2011.10.074.
- [38] Y. Ma, Q. Wang, B.B. Jiang, C.L. Li, J.M. Hao, X.N. Li, C. Dong, T.G. Nieh, Controlled formation of coherent cuboidal nanoprecipitates in body-centered cubic high-entropy alloys based on Al₂(Ni Co, Fe, C_{r)}14 compositions, Acta Mater. 147 (2018) 213–225, https://doi.org/10.1016/j.actamat.2018.01.050.
- [39] A.J. Ardell, Precipitation hardening, Metall Trans A 16A (1985) 1985–2135, https://doi.org/10.1016/B978-0-08-098204-5.00013-4.
- [40] J.A. Melander, On the critical resolved shear stress from misfitting particles, Scr. Metall. 12 (1978) 497–498, https://doi.org/10.1016/0001-6160(78)90127-x.
- [41] A. Melander, P.Å. Persson, The strength of a precipitation hardened AlZnMg alloy, Acta Metall. 26 (1978) 267–278, https://doi.org/10.1016/j. actamat.2018.01.050.
- [42] K.M. Youssef, A.J. Zaddach, C. Niu, D.L. Irving, C.C. Koch, A novel low-density, high-hardness, high-entropy alloy with close-packed single-phase nanocrystalline structures, Mat. Res. Lett. 3 (2015) 95-99. http://dx.doi.org/ 10.1080/21663831.2014.985855
- [43] M.C. Gao, D.B. Miracle, D. Maurice, X. Yan, Y. Zhang, J.A. Hawk, High-entropy functional materials, J. Mater. Res. 33 (19) (2018) 1–18, https://doi.org/ 10.1557/jmr.2018.323.
- [44] S. Aminorroaya Yamini, D.R.G. Mitchell, H. Wang, Z.M. Gibbs, Y. Pei, S.X. Dou, G.J. Snyder, Origin of resistivity anomaly in p-type leads chalcogenide multiphase compounds, AIP Adv. 5 (5) (2015) 053601, https://doi.org/10.1063/1.4913992.
- [45] H. Yang, K. Li, Y. Bu, J. Wu, Y. Fang, L. Meng, J. Liu, H. Wang, Nanoprecipitates induced dislocation pinning and multiplication strategy for designing high strength, plasticity and conductivity Cu alloys, Scr. Metall. 195 (2021) 113741, https://doi.org/10.1016/j.scriptamat.2021.113741.
- [46] T.M. Tritt, Recent trends in thermoelectric materials research, Chem. Phys. Carbon 31 (2000) 171–268.
- [47] Y. Zheng, S. Wang, W. Liu, Z. Yin, H. Li, X. Tang, C. Uher, Thermoelectric transport properties of p-type silver-doped PbS with in situ Ag₂S nanoprecipitates, J. Phys.: D 47 (2014) 323–328.
- [48] Q. Tan, L.-D. Zhao, J.-F. Li, C.-F. Wu, T.-R. Wei, Z.-B. Xing, M.G. Kanatzidis, Thermoelectrics with earth abundant elements: low thermal conductivity and high thermopower in doped SnS, J. Mater. Chem.: A 2 (41) (2014) 17302– 17306, https://doi.org/10.1039/C4TA04462B.

- [49] L.J. Zhang, J.T. Fan, D.J. Liu, M.D. Zhang, P.F. Yu, Q. Jing, M.Z. Ma, P.K. Liaw, G. Li, R.P. Liu, The microstructural evolution and hardness of the equiatomic CoCrCuFeNi high-entropy alloy in the semi-solid state, J. Alloys Compd. 745 (2018) 75–83. https://doi.org/10.1016/j.iallcom.2018.02.170.
- (2018) 75–83, https://doi.org/10.1016/j.jallcom.2018.02.170.

 [50] B. Poudel, Q. Hao, Y.i. Ma, Y. Lan, A. Minnich, B.o. Yu, X. Yan, D. Wang, A. Muto, D. Vashaee, X. Chen, J. Liu, M.S. Dresselhaus, G. Chen, Z. Ren, High-Thermoelectric Performance of Nanostructured Bismuth Antimony Telluride
- Bulk Alloys, Science 320 (5876) (2008) 634–638, https://doi.org/ 10.1126/science:1156446. [51] Y. Shi, B. Yang, X. Xie, J. Brechtl, K.A. Dahmen, P.K. Liaw, Corrosion of
- [51] Y. Shi, B. Yang, X. Xie, J. Brechtl, K.A. Dahmen, P.K. Liaw, Corrosion of Al_xCoCrFeNi high-entropy alloys: al-content and potential scan-rate dependent pitting behavior, Corros. Sci. 119 (2017) 33–45, https://doi.org/ 10.1016/j.corsci.2017.02.019.